A NUMERICAL MODEL ON COMPRESSIVE BEHAVIOR OF CFRP LAMINATE WITH A DESIGNED DELAMINATION

Xiangqian Zeng[1], Yi-Qi Wang[1*], Xueshu Liu[2] and Yongjie Bao[1], Hang Gao[1]

[1] Key Lab. for Precision and Non-traditional Machining Technology of Ministry of Education, School of Mechanical Engineering, Dalian University of Technology, Dalian 116024, China
(* E-mail: wangyiqi@dlut.edu.cn)
[2] School of Automotive Engineering, Dalian University of Technology, Dalian 116024, China

Keywords: Finite element, Compressive behavior, Cohesive element, Intralaminar failure, Delamination propagation

ABSTRACT

A progressive damage model based on extended Hashin criteria and cohesive model was developed to investigate the position effect of designed delamination on compressive behavior of CFRP laminate in thick direction. Designed delamination was placed in the CFRP laminate with different depths, which were varying from 1/20 to 10/20 of its thickness by considering the symmetry of laminate. Buckling mode, intralaminar failure, and the progress of designed delamination were obtained with the developed progressive damage model. As the designed delamination was embedded at depth position of 1/20, both local-buckling and global-buckling took place and the maximum local-buckling displacement reached 0.35 mm. While, only global-buckling occurred with designed delamination embedded at deeper position. Fiber tension and matrix crack usually generated at the outside of buckling laminate with only global-buckling while fiber compression and matrix crush inside. These four failure modes could be distinguished at local-buckling area of laminate which contained both local-buckling and global-buckling. The fiber direction of adjacent layers where designed delamination located was the predominant factor that affected the strength of laminate. Delamination propagated from the edge of designed delamination to free side with superficial designed delamination while the propagating path was opposite when the designed delamination was deeper.

1 INTRODUCTION

Composite laminates consisting of continuous carbon-fiber reinforced plies are now widely employed in engineering structures by the virtues of high strength and light weight. However, due to the lack of through-thickness reinforcement, delamination between two adjacent layers becomes one of the most serious damaging behaviors in laminated structures [1-4]. Delamination can be often pre-existing or generated during service life, which causes significant reductions in stiffness and strength. In particular, when the laminated composites are subjected to compressive loads, delamination usually originates from manufacturing flaws or interlaminar stress raises and propagates after initiation, which causes the degradation of the structural behavior and even catastrophic failure of the laminated structures [5]. It is therefore of great importance to understand the effect of delamination on the behavior of the composites.

Due to the high cost and impossibility to study each condition by experiment, various numerical methods have been gradually developed to assist the research of delamination problems. Among them, cohesive zone model (CZM) has been successfully adopted due to their high versatility and relative simplicity to be incorporated into research and commercial finite element (FE) codes. According to the original formulation of Dugdale [6] and Barenblatt [7], CZM hypothesizes a process (softening) zone located ahead of a crack tip where cohesive interactions, or tractions, are related to the interfacial separation, or displacement jump. Based on uniform constitutive relation to describe the crack initiation and propagation, CZM can avoid the stress singularity of crack tip in the linear elastic mechanics and is widely utilized by many researchers in the delamination analysis of composite [8]. A zero-thickness three dimensional cohesive element can commendably represent the buckling behavior and delamination growth in composite laminates with artificial and impact-induced delamination when

subject to four-point bending [9]. However, the influence of both the cohesive mesh size and the maximum tractions is sensitive when predicting the compressive behavior of damaged composite laminates [10]. Moreover, recommended guidelines have been provided for accurate simulations on the delamination growth in the multidirectional laminates [11]. In addition, Craven *et al.* [12] presented a FE model of carbon fiber reinforced plastics (CFRP) with multiple delaminations of realistic shape and including fiber fracture cracks loaded under compression, which showed that peanut shaped delaminations caused significant stiffness reduction and the contribution of fiber fracture cracks to further stiffness reduction was minimal but they had some significant effects on the buckling shapes. Therefore, the depth position effect of designed delamination on compressive failure modes and delamination propagation needs further study.

The main purpose is to investigate the effect of depth position of designed delamination on compressive behavior based on cohesive element method, simultaneously considering the failure modes of CFRP laminate. The results is implemented by standard ABAQUS software.

2 FINITE ELEMENT ANALYSIS

2.1 Failure criteria of constituents

ABAQUS/Standard [13] was used to develop numerical simulations of the CFRP laminate specimen with a designed delamination and taking account of the progressive development of damage. Hashin's failure criterion [14], which includes fiber failures and matrix cracks, has been widely employed to model the initiation of the damage. In order to overcome the shortcomings of Hashin's criterion, Dávila and Camanho [15] propose a new failure criterion, which is only suitable for in-plane stress conditions. However, as to describe the delamination phenomenon of laminated composite, the transfer of stress between layers cannot be negligible. Consequently, three-dimensional finite model was conducted and the initiation failure criteria with seven failure modes were adopted which were extended based on the four failure modes originally defined by Hashin, among which some indexes for predicting fiber and matrix failure were described in the following [16]:

Fiber tensile failure ($\sigma_{11} \geq 0$):

$$\left(\frac{\sigma_{11}}{X_T}\right)^2 + \frac{\tau_{12}^2/2G_{12} + 3\alpha\tau_{12}^4/4}{S_{12}^2/2G_{12} + 3\alpha S_{12}^4/4} + \frac{\tau_{13}^2/2G_{13} + 3\alpha\tau_{13}^4/4}{S_{13}^2/2G_{13} + 3\alpha S_{13}^4/4} = e_{ft}^2 \tag{1}$$

Fiber compressive failure ($\sigma_{11} < 0$):

$$\left(\frac{\sigma_{11}}{X_C}\right)^2 = e_{fc}^2 \tag{2}$$

In-plane matrix cracking ($\sigma_{22} \geq 0$):

$$\left(\frac{\sigma_{22}}{Y_T}\right)^2 + \frac{\tau_{12}^2/2G_{12} + 3\alpha\tau_{12}^4/4}{S_{12}^2/2G_{12} + 3\alpha S_{12}^4/4} + \frac{\tau_{23}^2/2G_{23} + 3\alpha\tau_{23}^4/4}{S_{23}^2/2G_{23} + 3\alpha S_{23}^4/4} = e_{imt}^2 \tag{3}$$

In-plane matrix crushing ($\sigma_{22} < 0$):

$$\left(\frac{\sigma_{22}}{Y_C}\right)^2 + \frac{\tau_{12}^2/2G_{12} + 3\alpha\tau_{12}^4/4}{S_{12}^2/2G_{12} + 3\alpha S_{12}^4/4} + \frac{\tau_{23}^2/2G_{23} + 3\alpha\tau_{23}^4/4}{S_{23}^2/2G_{23} + 3\alpha S_{23}^4/4} = e_{imc}^2 \tag{4}$$

where X_T and X_C represent tensile and compressive strengths in the fibre direction, Y_T and Y_C represent tensile and compressive strengths in the transverse direction, G and S represent the shear modulus and shear strengths. For composites with linear elastic behaviour, $\alpha = 0$.

The failure criteria can be used to judge the initial damage of composite constituents. Once the local damage occurs, the load-bearing capacity of laminate will decrease and with the damage growing the stiffness of material will decrease, thus leading to the load-bearing capacity gradually decrease to zero, which is a progressive damage process. The material stiffness degradation strategy used in this paper is based on the damage model proposed by McCarthy [17].

2.2 Cohesive zone method

The interface thickness of plies with different orientations is assumed to be negligibly small, so a

zero-thickness three-dimensional cohesive element is used to model the connection between each ply [12]. As shown in Fig. 1, based on bilinear traction-separation constitutive relationship, the top and bottom nodes of cohesive element are hold together using penalty stiffness K_N (Mode I) and K_S, K_T(Mode II and Mode III) in linear elastic range (Point 1). In pure Mode I, II or III loading condition, once the interfacial normal or shear tractions attain their respective interlayer tensile (*N*) or shear strengths (*S*, *T*) (Point 2), the stiffness of cohesive element will decrease. At this moment, if unloading happens the force and displacement will act as the line through point 3, in contrast if continuing the loading the force and displacement will act as line through point 4 until final damage in point 5. The areas under the traction-separation curves are equal to corresponding fracture toughness of each mode.

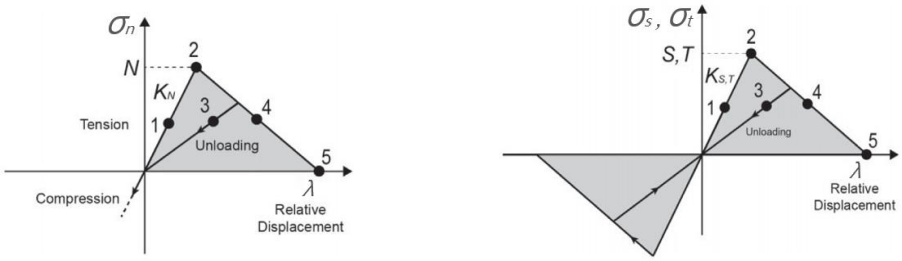

(a)Mode I (b) Mode II and Mode III

Fig. 1: Traction-separation constitutive relationship of cohesive model [18].

The stress status of composite under compression is complex and the delamination often occurs in mixed mode, a quadratic nominal stress criterion is employed to judge the initiation of delamination [19]:

$$\sqrt{\left(\frac{\langle \sigma_n \rangle}{N}\right)^2+\left(\frac{\sigma_s}{S}\right)^2+\left(\frac{\sigma_t}{T}\right)^2}=1 \tag{8}$$

where < > represents Macaulay bracket and signifies that a pure compressive deformation or stress state does not initiate delamination. σ_n, σ_s and σ_t are the normal stress and shear stresses on the interface; and *N*, *S* and *T* are the normal and shear strengths of interface.

The criteria used to predict delamination propagation under mixed-mode loading conditions are usually established in terms of the energy release rate and fracture toughness. The mixed-mode criterion proposed by Benzeggagh and Kenane [20] (B–K criterion) is competent to account for the variation of fracture toughness as a function of mode ratio in epoxy composites and is adopted in this paper, whose expression is as follows:

$$G_{IC}+\left(G_{IIC}-G_{IC}\right)\left\{\frac{G_{II}+G_{III}}{G_I+G_{II}+G_{III}}\right\}^{\eta}=G_C \tag{9}$$

where G_I , G_{II} and G_{III} are the strain energy release rate of mode I , II , and III . G_{IC} , G_{IIC} are the critical strain energy release rate (fracture toughness) in mode I , II .The parameter η can be obtained from MMB tests at different mode ratios, and in this paper it is set as 1.3.

2.3 Finite element modeling

The study of compressive behavior was carried out on an IMS194/CYCOM 977-2 carbon/epoxy laminate. The ratio of the CFRP laminate was W/L = 0.25, where W and L respectively present the width and the length of the CFRP laminate. To investigate the effect of depth position, a square designed delamination with size of 8 x 8 mm was embedded inside the laminate. The depth position of designed delamination was denoted with the ratio of top sub-laminate thickness *t* to laminate thickness T. A displacement-control compressive load was applied at the clamped end of the laminate while another two sides were free. A schematic representation of the CFRP laminate geometry was given in Fig. 2.

The laminate was assumed quasi-isotropic with a symmetrical stacking sequence of [45/90/-

45/0/90/0/-45/90/45/-45]s. The thickness of single ply was 0.188 mm. The lamina material properties and the interlaminar fracture properties used in the FE analyses were given in Table 1 and Table 2, respectively.

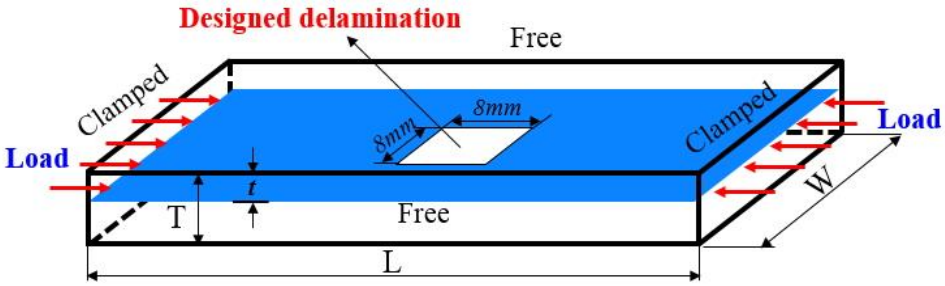

Fig. 2: The geometry, boundary condition and applied load of FE model.

E_{11} (GPa)	$E_{22} = E_{33}$ (GPa)	$G_{12} = G_{13}$ (GPa)	G_{23} (GPa)	$\nu_{12}=\nu_{13}$	ν_{23}
165	8.17	4.27	2.90	0.33	0.48
X_T (MPa)	X_C (MPa)	$Y_T = Z_T$ (MPa)	$Y_C = Z_C$ (MPa)	$S_{12}=S_{13}=S_{23}$ (MPa)	
3150	1450	81.4	270	108	

Table 1: Lamina elastic properties of CFRP laminate.

G_{IC} (N/mm)	$G_{IIC} = G_{IIIC}$ (N/mm)	N (MPa)	$S = T$ (MPa)	K_N (MPa/mm)	$K_S = K_T$ (MPa/mm)
0.276	0.807	30	50	30000	3000

Table 2: Interlaminar fracture properties of CFRP laminate.

The laminate was modeled using the eight-nodes 3D layered solid elements which can provide accurate interlaminate stresses and transverse shear effects effectively. Simultaneously, the interface between two sub-laminates was modeled by the eight-nodes 3D cohesive element with a zero thickness in order to predict delamination propagation.

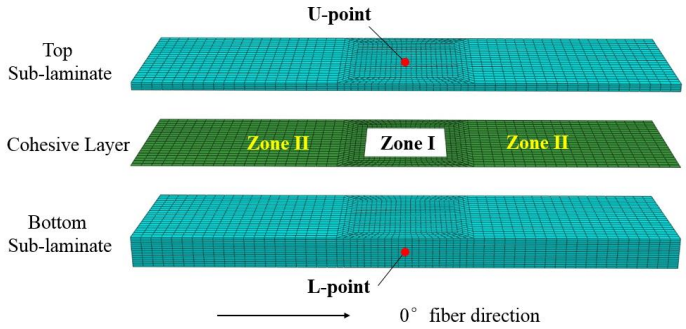

Fig. 3: FE model composed of top sub-laminate, cohesive layer, and bottom sub-laminate.

The structure of the sub-laminates and interface including designed delamination was presented in Fig. 3. The cohesive layer was inserted into sub-laminates (between top layer and bottom layer). All interface elements inside the delamination area (Zone I) were deleted as a numerical simulation of designed delamination and surface-to-surface contact element was placed to avoid penetration between plies, while the cohesive elements at Zone II remained. According to the empirical formula proposed by Rice and Falk et al. [21], a mesh size of 0.5mm is adequate to capture an accurate stress and strain

field in the cohesive zone while reducing the computational cost. The displacements of U-point (centre point of top sub-laminate) and L-point (centre point of bottom sub-laminate) along the thickness direction can effectively describe the delamination growth and buckling displacement of the laminate [22], and thus are obtained in this study.

3 RESULTS AND DISCUSSION

3.1 Modeling validation

To validate the accuracy of above FE method combining progressive damage and cohesion element, a FE model was implemented according to the geometry and material parameters given in the literature [23] and the obtained numerical results were compared with the experimental data of the literature. The comparison between experimental and numerical load–separate displacement curves were shown in Fig. 4. An excellent agreement between numerical prediction and experimental data was found in both buckling load and buckling displacement. The proposed FE method predicted the critical local-buckling load of 4186.1 N, similar to the experimental result of 4048.0 N, with an error less than 3.3%, while the error of load capacity obtained from numerical result of 10016.0 N and experimental data of 10005.5 N was only 0.1%. The maximum local-buckling displacement of numerical result was 0.30 mm, revealing an error of 6.25% comparing to the test data of 0.32 mm. Moreover, the present method can reproduce the non-linearity delamination propagation while considering the progressive failure of the laminate.

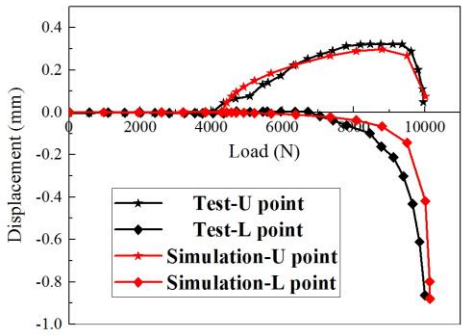

Fig. 4: Comparison of load-displacement behavior between test and simulation.

3.2 Buckling mode

In addition, the FE model was carried out to analyse the buckling mode with different depth position of designed delamination, as listed in Table.3. It was considered that the delaminated laminate was with constant square designed delamination of 8 mm x 8 mm, but various depth position from 1/20 to 10/20 due to the symmetry of laminate.

No.	Designed delamination (mm^2)	Depth position	Adjacent layers
1	8 x 8	1/20	45 ⁄90 °
2		2/20	90 ⁄-45 °
3		3/20	-45 ⁄0 °
4		4/20	0 ⁄90 °
5		6/20	0 ⁄-45 °
6		8/20	90 ⁄45 °
7		10/20	-45 ⁄-45 °

Table 3: Depth position configuration of designed delamination.

As was shown in Fig. 5, when the designed delamination was embedded at depth position of 1/20, both local-buckling and global-buckling existed and the maximum local-buckling displacement reached 0.35 mm (seen in Fig. 6 (a)), nevertheless, only global-buckling took place as it was imbedded

at deeper position, which could be explained by the stronger suppression of adjacent sub-laminate with thicker sub-laminate. Furthermore, when the designed delamination was at the center depth, the buckling displacement was only 0.005 mm, while the local-buckling and global-buckling occurred at the same time and was symmetrical to each other, as illustrated in Fig. 6 (e). When the designed delamination was at the center of laminate, the top and bottom sub-laminate were same and the suppression was strongest, thus only a small strength reduction.

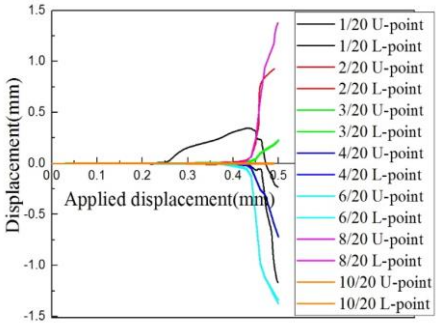

Fig. 5: Buckling displacement behavior with different depth position.

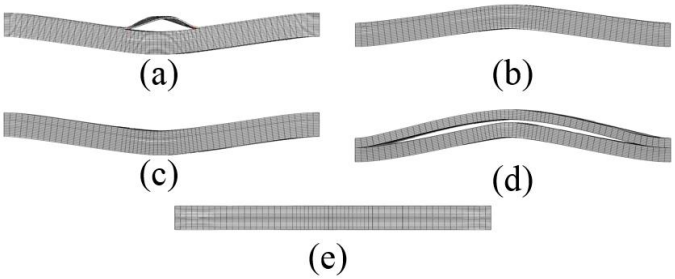

Fig. 6: Buckling mode with different depth position: (a) 1/20, (b) 3/20, (c) 6/20, (d) 8/20, (e) 10/20.

3.3 Intralaminar failure

Based on progressive damage method, the intralaminar failure mode with different depth position was obtained and the effect on the strength of laminate was evaluated. The strength of laminate with designed delamination at center depth was the biggest while a serious decline of 10.70 MPa arouse with delamination at depth position of 1/20, as was shown in Fig. 7. It indicated that the designed delamination played a significant role in strength decrease when it was superficial. Moreover, serious reduction of strength also took place at depth position of 2/20 and 8/20, with 9.24 MPa and 10.43 MPa, whose adjacent layers' fiber directions were 90 °/-45 ° and 90 °/45 °. Combining with the fiber directions of adjacent layer at depth position 1/20 which were 45 °/90 °, the reason was properly that 90 ° layer didn't bear load as the compressive load was longitudinal.

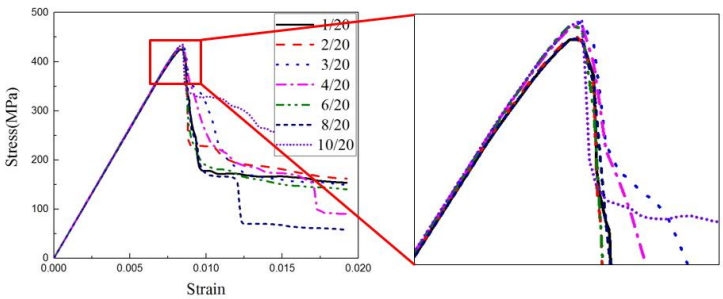

Fig. 7: The effect of depth position on stress-strain curves.

The result of intralaminar failure which was accessed by extended Hashin criteria was attained, including fiber tension, fiber compression, matrix crack and matrix crush, as illustrated in Fig. 8. It was clearly that these four failure modes occurred at the local-buckling area of delaminated laminate with designed delamination at depth position of 1/20. However, at deeper position, due to global-buckling only, fiber tension and matrix crack usually took place at outside of buckling laminate while fiber compression and matrix crush inside. It was because of compressive stress inside and tensile stress outside the buckling laminate when subjected to compressive load. Matrix failed more easily than fiber as its strength was lower. In addition, failure took place preferentially at fixed end when there was designed delamination at the center of laminate, revealing that it could be acceptant if only small delamination existed away from the edge of laminate.

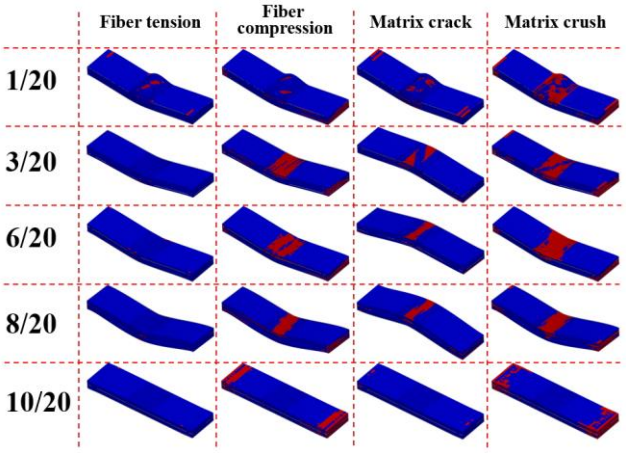

Fig. 8: Intralaminar failure of different depth position.

3.4 Delamination

Fig. 9 showed the delamination propagation of delaminated laminate with depth position of 1/20, 3/20, 6/20, 8/20 and 10/20, respectively. At depth position of 1/20, delamination propagated transverse from the edge of designed delamination to free side and a through-the-width delamination formed. After that, it grew along loading direction and failed at last, thus local-buckling occurred easily. However, delamination always grew from free side of the laminate with deeper designed delamination, in spite of through-the-width delamination generated at depth position of 6/20 and 8/20. What's more, delamination propagation was difficult to occur with center designed delamination. It demonstrated that depth position made a big difference in delamination growth, including propagating path and delamination area.

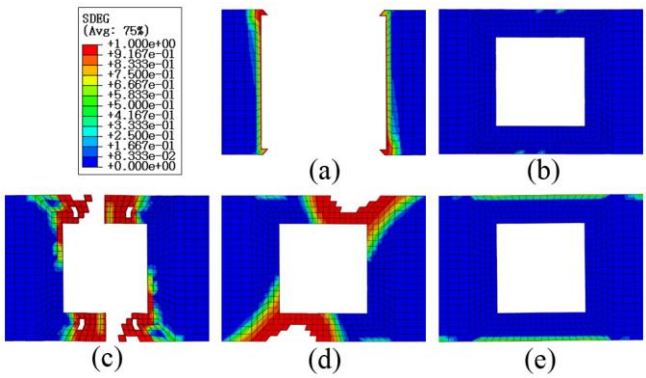

Fig. 9: Delamination propagation with different depth position:
(a) 1/20, (b) 3/20, (c) 6/20, (d) 8/20, (e) 10/20.

4 CONCLUSIONS

A progressive damage model was developed based on extended Hashin criteria and cohesive model. To investigate the depth position effect of designed delamination on compressive behavior of CFRP laminate in thick direction, designed delamination was embedded in the symmetrical CFRP laminate with different depths, varying from 1/20 to 10/20 of its thickness. Based on the developed progressive damage model, buckling mode, intralaminar failure, and the growth of designed delamination were obtained and summarised as follows:

(1) When the designed delamination was embedded at depth position of 1/20, both local-buckling and global-buckling existed and the maximum local-buckling displacement reached 0.35 mm, nevertheless, only global-buckling took place as it was imbedded at deeper position. Moreover, when the designed delamination was at the center depth, the local-buckling and global-buckling occurred at the same time and was symmetrical to each other with only 0.005mm buckling displacement.

(2) The strength of laminate with designed delamination at center depth was the biggest while it declined severely when the fiber direction of adjacent layer where designed delamination located contained 90°. When local-buckling existed, failure easily generated at the local-buckling area. However, as for only global-buckling, fiber tension and matrix crack usually took place at outside of buckling laminate while fiber compression and matrix crush inside.

(3) Depth position made a big difference in delamination growth, including propagating path and delamination area. At depth position of 1/20, delamination propagated transverse from the edge of designed delamination to free side and a through-the-width delamination formed. After that, it grew along loading direction and failed at last, thus local-buckling occurred easily. However, delamination always grew from free side of the laminate with deeper designed delamination, and the delamination area was relatively decreased.

ACKNOWLEDGEMENTS

This work was supported by the National Natural Science Foundation of China (Grant No. 51375068, Grant No. 51475073, and Grant No. 51605076), the National Key Basic Research Program of China (Grant No. 2014CB046504), and the Liaoning Province Natural Science Foundation (Grant No. 201602171).

REFERENCES

[1] D.J. Mortell, D.A. Tanner and C.T. McCarthy, In-situ SEM study of transverse cracking and delamination in laminated composite materials, *Composites Science and Technology*, **105**, 2014, pp. 118-126(doi: 10.1016/j.compscitech.2014.10.012).

[2] C. Canturri, E.S. Greenhalgh and S.T. Pinho, The relationship between mixed-mode II/III delamination and delamination migration in composite laminates, *Composites Science and Technology*, **105**, 2014, pp. 102-109(doi: 10.1016/j.compscitech.2014.10.001).

[3] L.B. Zhao, Y. Gong, J.Y. Zhang, Y.L. Chen and B.J. Fei, Simulation of delamination growth in multidirectional laminates under mode I and mixed mode I/II loadings using cohesive elements, *Composite Structures*, **116**, 2014, pp. 509-522(doi: 10.1016/j.compstruct.2014.05.042).

[4] A.M. Elmarakbi, N. Hu and H. Fukunaga, Finite element simulation of delamination growth in composite materials using LS-DYNA, *Composites Science and Technology*, **69**, 2009, pp. 2383-2391(doi: 10.1016/j.compscitech.2009.01.036).

[5] H.R. Ovesy and M. Kharazi, Compressional stability behavior of composite plates with through-the-width and embedded delaminations by using first order shear deformation theory, *Computers & Structures*, **89**, 2011, pp. 1829-1839(doi: 10.1016/j.compstruc.2010.10.016).

[6] D.S. Dugdale, Yielding Of Steel Sheets Containing Slits, *Journal of the Mechanics and Physics of Solids*, **8**, 1960, pp. 100-104(doi: 10.1016/0022-5096(60)90013-2).

[7] G.I. Barenblatt, Citation Classic - the Mathematical-Theory Of Equilibrium Cracks In Brittle-Fracture, *Current Contents/Engineering Technology & Applied Sciences*, 1983, pp. 20-20.

[8] D. Feng and F. Aymerich, Finite element modelling of damage induced by low-velocity impact on composite laminates, *Composite Structures*, **108**, 2014, pp. 161-171(doi: 10.1016/j.compstruct.2013.09.004).
[9] W.R. Gong, J.L. Chen and E.A. Patterson, Buckling and delamination growth behaviour of delaminated composite panels subject to four-point bending, *Composite Structures*, **138**, 2016, pp. 122-133(doi: 10.1016/j.compstruct.2015.11.054).
[10] E. Panettieri, D. Fanteria and F. Danzi, Delaminations growth in compression after impact test simulations: Influence of cohesive elements parameters on numerical results, *Composite Structures*, **137**, 2016, pp. 140-147(doi: 10.1016/j.compstruct.2015.11.018).
[11] L.B. Zhao, Y. Gong, J.Y. Zhang, Y.L. Chen and B.J. Fei, Simulation of delamination growth in multidirectional laminates under mode I and mixed mode I/II loadings using cohesive elements, *Composite Structures*, **116**, 2014, pp. 509-522(doi: 10.1016/j.compstruct.2014.05.042).
[12] R. Craven, L. Iannucci and R. Olsson, Delamination buckling: A finite element study with realistic delamination shapes, multiple delaminations and fibre fracture cracks, *Composites: Part A*, **41**, 2010, pp. 684-692(doi: 10.1016/j.compositesa.2010.01.019).
[13] Abaqus Inc., *Abaqus Documentation, Version 6.13*, Dassault Systèmes SIMULIA Corporation, Providence, 2013.
[14] Z. Hashin, Failure Criteria for Unidirectional Fiber Composites, *Journal of Applied Mechanics-Transactions of the ASME*, **47**, 1980, pp. 329-334.
[15] C.G Davila, N. Jaunky and S. Goswami, Failure Criteria for FRP Laminates in Plane Stress, *the 44th AIAA/ASME/ASCE/AHS Structures, Structural Dynamics, and Materials Conference, Norfolk, Virginia, April 7-10, 2003*, American Institute of Aeronautics and Astronautics, 2003, pp. 1-11(doi: 10.2514/6.2003-1991).
[16] A. Olmedo and C. Santiuste, On the prediction of bolted single-lap composite joints, *Composite Structures*, **94**, 2012, pp. 2110-2117(doi: 10.1016/j.compstruct.2012.01.016).
[17] C.T. McCarthy, R.M. O'Higgins and R.M. Frizzell, A cubic spline implementation of non-linear shear behaviour in three-dimensional progressive damage models for composite laminates, *Composite Structures*, **92**, 2010, pp. 173-181(doi: 10.1016/j.compstruct.2009.07.025).
[18] X.F. Lou, H.N. Cai, P.F. Yu, F. Jiao and X.C. Han, Failure analysis of composite laminate under low-velocity impact based on micromechanics of failure, *Composite Structures*, **163**, 2017, pp. 238-247(doi: 10.1016/j.compstruct.2016.12.030).
[19] P.P. Camanho, C.G. Davila and M.F. de Moura, Numerical simulation of mixed-mode progressive delamination in composite materials, *Journal of Composite Materials*, **37**, 2003, pp. 1415-1438(doi: 10.1177/002199803034505).
[20] M.L. Benzeggagh and M. Kenane, Measurement of mixed-mode delamination fracture toughness of unidirectional glass/epoxy composites with mixed-mode bending apparatus, *Composites Science and Technology*, **56**, 1996, pp. 439-449(doi: 10.1016/0266-3538(96)00005-X).
[21] M.L. Falk, A. Needleman and J.R. Rice, A critical evaluation of cohesive zone models of dynamic fracture, *Journal De Physique Iv*, **11**, 2001, pp. 43-50(doi: 10.1051/Jp4:2001506).
[22] N. Kharghani and C.G. Soares, Behavior of composite laminates with embedded delaminations, *Composite Structures*, **150**, 2016, pp. 226-239(doi: 10.1016/j.compstruct.2016.04.042).
[23] L. Zhang, Numerical analysis and experimental study on propagation behavior of laminated composite plates with embedded delamination, *Harbin Institute of Technology*, *PhD thesis*, May, 2012.